

# A novel parallel-rotation algorithm for atomistic Monte Carlo simulation of dense polymer systems

S. Santos and U. W. Suter

*Department of Materials, Institute of Polymers, Eidgenössische Technische Hochschule (ETH),  
Zürich, Switzerland*

M. Müller and J. Nievergelt

*Department of Computer Science, Institute of Theoretical Computer Science, Eidgenössische Technische  
Hochschule (ETH), Zürich, Switzerland*

(Received 27 October 1998; accepted 22 March 2001)

We develop and test a new elementary Monte Carlo move for use in the off-lattice simulation of polymer systems. This novel **Parallel-Rotation** algorithm (ParRot) permits moving very efficiently torsion angles that are deeply inside long chains in melts. The parallel-rotation move is extremely simple and is also demonstrated to be computationally efficient and appropriate for Monte Carlo simulation. The ParRot move does not affect the orientation of those parts of the chain outside the moving unit. The move consists of a concerted rotation around four adjacent skeletal bonds. No assumption is made concerning the backbone geometry other than that bond lengths and bond angles are held constant during the elementary move. Properly weighted sampling techniques are needed for ensuring detailed balance because the new move involves a correlated change in four degrees of freedom along the chain backbone. The ParRot move is supplemented with the classical Metropolis Monte Carlo, the Continuum-Configurational-Bias, and Reptation techniques in an isothermal-isobaric Monte Carlo simulation of melts of short and long chains. Comparisons are made with the capabilities of other Monte Carlo techniques to move the torsion angles in the middle of the chains. We demonstrate that ParRot constitutes a highly promising Monte Carlo move for the treatment of long polymer chains in the off-lattice simulation of realistic models of dense polymer systems.

© 2001 American Institute of Physics. [DOI: 10.1063/1.1371496]

## I. INTRODUCTION

In dense polymer systems in continuous space, the goal of efficient phase-space sampling by Monte Carlo (MC) is a most difficult one, since it is very hard in simulations to change from one configuration to the successive one, especially at high densities. Significant progress has been made in this field in the last few years by a combination of geometric methods such as Reptation,<sup>1-3</sup> the Continuum-Configurational-Bias method (CBMC),<sup>4-6</sup> or the Concerted-Rotation method<sup>7,8</sup> and its extensions.<sup>9</sup>

Here we introduce a novel off-lattice sampling technique that aims at enhancing the efficiency of existing MC methods. We focus our attention on three currently incompatible aspects essential for the new algorithm to be a prerequisite for a promising sampling technique: the computational efficiency and robustness, the ability to treat long polymer chains, and the applicability to chemically realistic polymer structures with side-groups.

The new elementary move, a Parallel-Rotation algorithm (ParRot), consists of a concerted rotation around four adjacent skeletal bonds forming the moving unit in such a way that the orientation of those parts of the chain outside the moving unit is not modified.

In this paper, the ParRot move is supplemented with the classical Metropolis Monte Carlo (MMC), the Continuum-Configurational-Bias, and Reptation techniques in

isothermal-isobaric Monte Carlo simulations of melts of short and long chains.

## II. THE PARALLEL ROTATION ALGORITHM

The high-dimensionality of the configurational space to sample constitutes a major difficulty in simulations of dense polymer phases. Fortunately, the structural complexity of polymeric systems, namely, the geometry and connectivity, provides a way to simplify the problem: by working in generalized coordinates, the number of degrees of freedom may be considerably reduced.<sup>10</sup> The molecular geometry can be solely determined by the position and orientation of the chain start and by the successive torsion angles along the backbone. The bond length and the bond angles are assumed to be fixed (truly rigid constraint bonds). This assumption only slightly affects the vibrational frequencies of the “soft” modes associated with torsion angles.<sup>11</sup> Since the approach is designed to be used in configuration-space Monte Carlo methods, only the potential energy part of the system Hamiltonian is addressed.

### A. The geometric problem

The rearrangement of dihedral angles of a chain in a concerted fashion, subsequent to the turning of one single dihedral angle, has been first addressed by Go and Scheraga,<sup>7</sup> and further developed by Dodd, Boon, and Theodorou<sup>8</sup> as the Concerted-Rotation method (ConRot).

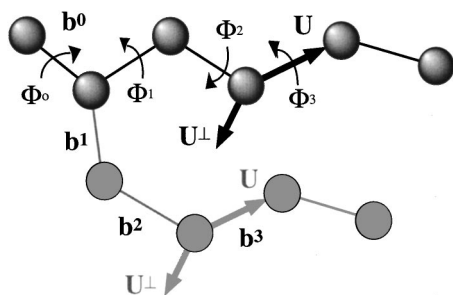


FIG. 1. The ParRot move is a concerted change in the torsion angles  $\{\phi_1, \phi_2, \phi_3\}$  driven by a change in  $\phi_0$ . The vectors  $\mathbf{u}$  and  $\mathbf{u}_\perp$  remain unchanged after the ParRot move.

The ParRot move consists of a concerted rotation of an arbitrary set of four adjacent torsion angles within a chain. These torsion angles form a moving unit that, in the same way as a hinge, determines the relative position and orientation of both the chain ends attached to it. The ParRot move is a rearrangement of the dihedral angles within that moving unit, whereas both chain ends attached to it are coerced to keep the same relative orientation (but not the same relative position). In other words, if one of the chain ends is kept fixed in space, the other chain end is displaced but its orientation remains unchanged.

Imposing a constant orientation to chain ends involves three geometric constraints, two for the direction and one for the orientation along this direction. To fulfill three conditions, the ParRot move must, at least, comprise the concerted move of three degrees of freedom. The fourth dihedral angle, the driver torsion angle, serves to steer the concerted move.

Consider the four contiguous bonds with torsion angles  $\{\phi_0, \phi_1, \phi_2, \phi_3\}$  in Fig. 1 to form the ParRot moving unit. The rotation bond  $\mathbf{b}_3$  with the torsion angle  $\phi_3$  defines the direction of the chain end attached to the moving unit. The vector  $\mathbf{b}_2 \times \mathbf{b}_3$  furthermore determines its orientation. Throughout this paper, we use the unit vectors  $\mathbf{u}(\parallel \mathbf{b}_3)$  and  $\mathbf{u}_\perp(\parallel \mathbf{b}_2 \times \mathbf{b}_3)$  as direction and orientation vectors, respectively. The ParRot move keeps  $\mathbf{u}$  and  $\mathbf{u}_\perp$  constant.

We use  $\mathbf{T}(\phi)$  to define the transformation of a vector in the frame of reference of bond  $i+1$  into the frame of the preceding bond  $i$  (see Fig. 2), expressed as the combination of two rotations,<sup>12</sup>

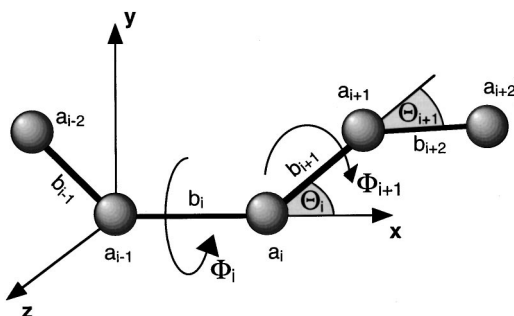


FIG. 2. Generalized Coordinates encompass torsion angles along the backbone. The bond angle supplements  $\theta_i$  and the bond lengths  $\|\mathbf{b}_i\|$  are assumed to be fixed. In the local coordinate system located at each atom  $\mathbf{a}_{i-1}$ , the bond vector  $\mathbf{b}_i$  is aligned along the local x-axis ( $\mathbf{e}_x$ ).

$$\mathbf{T}(\phi) = \mathbf{R}_x(\phi) \mathbf{R}_z(\pi + \theta)$$

$$= \begin{bmatrix} -\cos \theta & \sin \theta & 0 \\ -\cos \phi \sin \theta & -\cos \phi \cos \theta & -\sin \phi \\ -\sin \phi \sin \theta & -\sin \phi \cos \theta & \cos \phi \end{bmatrix}. \quad (1)$$

Note that the bond angle  $\theta$  must not necessarily be the same for all bond junctions along the skeletal chain backbone.

As previously suggested, the geometric constraint for a parallel rotation (ParRot) move is that both vectors  $\mathbf{u}$  and  $\mathbf{u}_\perp$  are kept constant. A system of two equations, dictated by the molecular geometry, to account for the geometric constraints can now be specified in the reference frame of the bond vector  $\mathbf{b}_0$  as

$$\begin{aligned} \mathbf{u} &= \mathbf{T}(\phi_0^{\text{driver}}) \mathbf{T}(\phi_1^{\text{new}}) \mathbf{T}(\phi_2^{\text{new}}) \mathbf{e}_x \\ &= \mathbf{T}(\phi_0) \mathbf{T}(\phi_1) \mathbf{T}(\phi_2) \mathbf{e}_x, \end{aligned} \quad (2)$$

$$\begin{aligned} \mathbf{u}_\perp &= \mathbf{T}(\phi_0^{\text{driver}}) \mathbf{T}(\phi_1^{\text{new}}) \mathbf{T}(\phi_2^{\text{new}}) \mathbf{T}(\phi_3^{\text{new}}) \mathbf{e}_y \\ &= \mathbf{T}(\phi_0) \mathbf{T}(\phi_1) \mathbf{T}(\phi_2) \mathbf{T}(\phi_3) \mathbf{e}_y, \end{aligned} \quad (3)$$

where  $\phi_0^{\text{driver}}$  denotes the new value imposed for the driver torsion angle, and  $\{\phi_1^{\text{new}}, \phi_2^{\text{new}}, \phi_3^{\text{new}}\}$  the new values of the remaining angles of the moving unit to be determined. As a matter of fact, these six scalar equations enforce only three implicit geometric constraints to be fulfilled. This is due to the fact that  $\mathbf{T}$ , as a rotation in space, conserves the vector lengths, and, therefore, the vectors  $\mathbf{u}$  and  $\mathbf{u}_\perp$  automatically have the same length as the vectors  $\mathbf{e}_x$  and  $\mathbf{e}_y$  (of unit length). In addition, because of the same reason, the vectors  $\mathbf{u}$  and  $\mathbf{u}_\perp$ , which are, by definition, perpendicular, and consequently not independent, are necessarily mapped back onto a pair of perpendicular vectors. The vectors  $\mathbf{e}_x$  and  $\mathbf{e}_y$  are perpendicular, and, so, an additional constraint is implicitly satisfied. To sum up, the vector  $\mathbf{u}$  accounts for the conservation of direction of the moving chain end, and the vector  $\mathbf{u}_\perp$  for its orientation along  $\mathbf{u}$ .

Since Eq. (2) and (3) involve four degrees of freedom and only three constraints, the system of equation is under-determined. One of the dihedral degrees of freedom can be freely chosen to determine the values of the others, i.e., the ParRot move is uniquely driven by a change of  $\phi_0$  into  $\phi_0^{\text{driver}}$ .

Solving Eq. (2) directly provides the value  $\phi_2$  of the second torsion angle. To calculate  $\phi_2$ , first consider the vector

$$\mathbf{v}(\phi_0^{\text{driver}}, \phi_0, \phi_1, \phi_2) := \mathbf{T}(\phi_0^{\text{driver}})^{-1} \mathbf{u}(\phi_0, \phi_1, \phi_2), \quad (4)$$

which is entirely determined by the known values  $\phi_0^{\text{driver}}$ ,  $\phi_0$ ,  $\phi_1$ , and  $\phi_2$ . The component  $v_x$  solely depends on the new value  $\phi_2^{\text{new}}$ , and consequently directly provides the solution

$$\cos \phi_2^{\text{new}} = \frac{\cos \theta_1 \cos \theta_2 - v_x(\phi_0^{\text{driver}}, \phi_0, \phi_1, \phi_2)}{\sin \theta_2 \sin \theta_1}, \quad (5)$$

where  $\theta_1$  and  $\theta_2$  are the bond angles between bonds  $\mathbf{b}_1$  and  $\mathbf{b}_2$ , and bonds  $\mathbf{b}_2$  and  $\mathbf{b}_3$ , respectively. According to the

value of the right-hand side in Eq. (5),  $\phi_2^{\text{new}}$  admits either zero (r.h.s. > 1), one (r.h.s. = 1) or two values (r.h.s. < 1).

Upon substituting the obtained values for  $\phi_2^{\text{new}}$  into Eq. (3), one gets the linear equation,

$$\begin{bmatrix} \cos \phi_1^{\text{new}} \\ \sin \phi_1^{\text{new}} \end{bmatrix} = \begin{bmatrix} a & -b \\ b & a \end{bmatrix} \frac{1}{1 - \mathbf{v}_x^2} \begin{bmatrix} \mathbf{v}_y \\ \mathbf{v}_z \end{bmatrix}, \quad (6)$$

where the parameters  $a := (\sin \theta_1 \cos \theta_2 + \cos \phi_2^{\text{new}} \times \cos \theta_1 \sin \theta_2)$  and  $b := (\sin \theta_2 \sin \phi_2^{\text{new}})$  depend upon  $\phi_2^{\text{new}}$ . The fact that  $a^2 + b^2 = 1$  indicates that the matrix in Eq. (6) is a rotation matrix, and hence conserves the vector lengths. This is in complete agreement with the fact that the left-hand side of Eq. (6) is a vector of unit length and that  $\mathbf{v}_y^2 + \mathbf{v}_z^2 = 1 - \mathbf{v}_x^2$  holds. Thus, we can conclude that, for each value of  $\phi_2^{\text{new}}$ , a unique solution  $\phi_1^{\text{new}}$  exists.

While the dihedral angles  $\phi_0$ ,  $\phi_1$ , and  $\phi_2$  suffice to determine the direction vector  $\mathbf{u}$ , the remaining degree of freedom  $\phi_3$  only causes the vector  $\mathbf{u}_\perp$  to be rotated around  $\mathbf{u}$ . Given the three first torsion angles,  $\phi_3^{\text{new}}$  can readily be calculated as the angle between  $\mathbf{u}_\perp$  and the corresponding vector when  $\phi_3$  has not yet been modified.

The ParRot move can be summarized as the following steps: (i) a driver torsion angle  $\phi_0$  is selected within the chain; (ii) one of the two chain ends starting from  $\phi_0$  is selected and the orientation vectors  $\mathbf{u}$  and  $\mathbf{u}_\perp$  are calculated; (iii) a value  $\phi_0^{\text{new}}$  is assigned to the driver torsion angle; (iv) sets of new values  $\phi_1^{\text{new}}$ ,  $\phi_2^{\text{new}}$ , and  $\phi_3^{\text{new}}$  for the three torsion angles  $\phi_1$ ,  $\phi_2$ ,  $\phi_3$  consecutive to  $\phi_0$  on the side of the selected chain end are calculated so that  $\mathbf{u}$  and  $\mathbf{u}_\perp$  remain unchanged. In this formulation,  $\phi_0$  is the driver torsion angle of the ParRot move. Only the four dihedral angles  $\{\phi_0, \phi_1, \phi_2, \phi_3\}$  are modified by the move.

## B. The ParRot move

At first sight, it is not obvious whether the ParRot technique can successfully handle long polymer chains in a dense phase. As one might expect, the critical factor for moves of chain segments to be at all feasible in a dense environment is the amplitude of displacement of atoms induced by the move. In the case of ParRot, because of the conservation of its orientation, the displacement of a chain end is such that all involved atoms are displaced by the same vector. The displacement amplitude determines if severe overlaps between atoms are likely to occur in a Monte Carlo simulation.

Figure 3 shows a typical ParRot trajectory for values of the driver angle  $\phi_0$  ranging from 0 to  $2\pi$ . The bond angle complements all assume the same value  $\theta = 68^\circ$  corresponding to the ‘‘polybead’’ model used later for Monte Carlo simulations. The bond length is 1.53 Å, and the van der Waals radius  $\sigma = 3.94$  Å gives an estimate of the typical distance between closest atoms. It is fortunate that, despite large changes in the dihedral angles involved in the ParRot move, the displacements in space of the atoms from their original positions is almost always small compared to  $\sigma$ . Half the  $\phi_0$  values (in our example, from 0 to  $0.3\pi$  and  $1.3\pi$  to  $2\pi$ ) induce at least one displacement smaller than 1 Å. This example strongly suggests that, even in simulations of dense phases, large concerted changes in  $\phi_1$ ,  $\phi_2$ , and  $\phi_3$  associ-

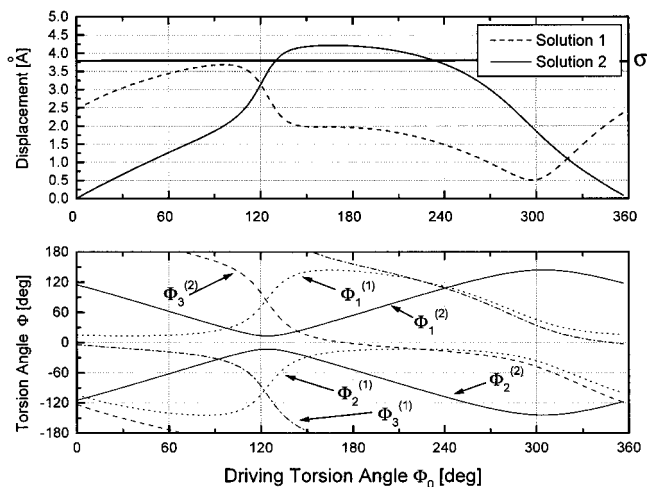


FIG. 3. The displacements of the moving chain end are shown for the two solutions of the ParRot problem for varying  $\phi_0 \in [0, 2\pi]$  with initial values of the torsion angles of  $\phi_0 = 0^\circ$ ,  $\phi_1 = 15^\circ$ ,  $\phi_2 = 115^\circ$ , and  $\phi_3 = -4^\circ$ . Comparison is made with the van der Waals radius,  $\sigma = 3.94$  Å. The corresponding sets  $\{\phi_1, \phi_2, \phi_3\}$  of solutions are also shown.

ated with large changes in  $\phi_0$  are possible without inducing large atom displacements, and thus without creating severe overlaps. This must also hold for torsion angles deeply within long polymer chains.

## C. A bias Monte Carlo

Turning to Monte Carlo simulations requires the indispensable detailed-balance condition to hold in order to ensure the distribution to be stationary along the Monte Carlo simulation.<sup>13</sup> This, in turn, requires the exact number of solutions for a Monte Carlo move to be known. As discussed by Dodd *et al.*,<sup>8</sup> and Leontidis *et al.*,<sup>9</sup> the Concerted Rotation algorithm, which also consists of a concerted move of dihedral angles driven by the changes in one driver angle, necessitates challenging numerical calculations to estimate the number of solutions. On the contrary, the existence of an analytical solution for the ParRot algorithm permits us to exactly calculate the number of solutions for any attempts of ParRot moves. The ParRot algorithm does not pose any numerical problems that could endanger its efficiency.

A proper choice of the acceptance criterion (for instance Metropolis or Glauber dynamics) guarantees a stationary ensemble distribution, which can be, for instance, the Gibbs ensemble distribution. In this case, the Monte Carlo acceptance probability for going from state  $n$  to  $m$ ,

$$P(n \rightarrow m) = \min \left\{ 1, \frac{N(m \rightarrow n) J(n) \exp[-\beta V(n)]}{N(n \rightarrow m) J(m) \exp[-\beta V(m)]} \right\} \quad (7)$$

suffices, where  $\beta := (k_b T)^{-1}$ , and  $V(n)$  is the potential energy of the state labeled with  $n$ .  $N(n \rightarrow m)$  is the total number of states attainable from  $n$  in the move leading from state  $n$  to  $m$ .  $J(n)$  is the Jacobian determinant factor, which has been introduced in the acceptance probability in Eq. (7) to counterbalance the geometric bias.

A Monte Carlo method that simultaneously encompasses several degrees of freedom in a concerted manner usually generates biased distributions of states, if not corrected. The

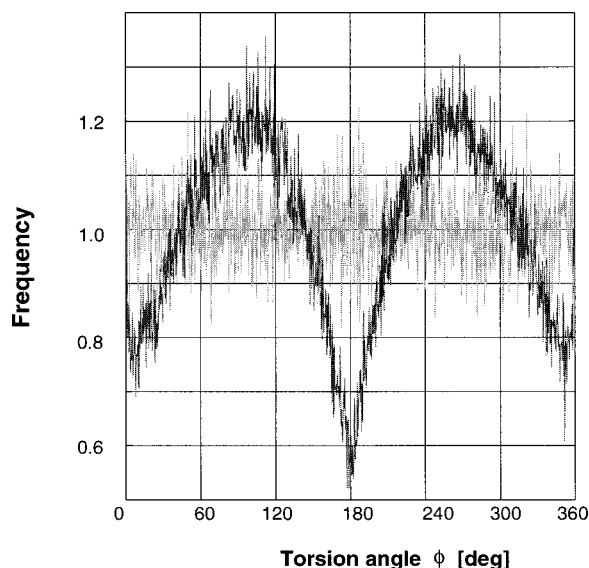


FIG. 4. Torsion angle distribution in a Monte Carlo simulation of  $C_{10}$  phantom chains. The black curve has been obtained in simulation without Jacobian bias correction  $J(n)$  in the acceptance probability, and the gray curve corresponds to simulation with Jacobian bias correction.

Monte Carlo acceptance scheme must be biased to provide the correct uniform distribution corresponding to  $V(n)$ , i.e., proportional to the Boltzmann weight of  $V(n)$ . Following Dodd *et al.*,<sup>8</sup> we calculate  $J(n)$  as Jacobian determinant of a transformation relating the coordinate frame of geometric constraints  $\mathbf{u}$  and  $\mathbf{u}_\perp$  to the one of dihedral angles  $\{\phi_0, \phi_1, \phi_2, \phi_3\}$ . We define

$$J(\phi_0, \mathbf{u}, \mathbf{u}_\perp) := \det \begin{bmatrix} \frac{\partial \mathbf{u}}{\partial \phi_1} \cdot \mathbf{e}_\lambda & \frac{\partial \mathbf{u}}{\partial \phi_2} \cdot \mathbf{e}_\lambda & \frac{\partial \mathbf{u}}{\partial \phi_3} \cdot \mathbf{e}_\lambda \\ \frac{\partial \mathbf{u}}{\partial \phi_1} \cdot \mathbf{e}_\gamma & \frac{\partial \mathbf{u}}{\partial \phi_2} \cdot \mathbf{e}_\gamma & \frac{\partial \mathbf{u}}{\partial \phi_3} \cdot \mathbf{e}_\gamma \\ \frac{\partial \mathbf{u}_\perp}{\partial \phi_1} \cdot \mathbf{e}_\eta & \frac{\partial \mathbf{u}_\perp}{\partial \phi_2} \cdot \mathbf{e}_\eta & \frac{\partial \mathbf{u}_\perp}{\partial \phi_3} \cdot \mathbf{e}_\eta \end{bmatrix}, \quad (8)$$

where  $\eta, \lambda, \gamma \in \{x, y, z\}$ , and  $\lambda \neq \gamma$ .

A change in torsion angle  $\phi_i$  is tantamount to a rotation about the backbone bond  $\mathbf{b}_i$ , that only affects the bonds  $\mathbf{b}_j$ , where  $j > i$ . The infinitesimal rotation about  $\mathbf{b}_i$  may be written as

$$\frac{\partial \mathbf{b}_j}{\partial \phi_i} = \begin{cases} 0 & j \leq i, \\ \mathbf{b}_i \times \mathbf{b}_j & j > i. \end{cases} \quad (9)$$

Substituting Eq. (2.3) in Eq. (8) leads to the final expression,

$$J(\phi_0, \mathbf{u}, \mathbf{u}_\perp) \propto |\mathbf{u} \cdot (\mathbf{u}_1 \times \mathbf{u}_2)|, \quad (10)$$

where the vectors  $\mathbf{u}_i := \mathbf{b}_i / \|\mathbf{b}_i\|$  of unit length are collinear to  $\mathbf{b}_1$  and  $\mathbf{b}_2$ , the bonds with torsion angles  $\phi_1$  and  $\phi_2$ , respectively. To determine the acceptance probability of a Monte Carlo move,  $J(n)$  must be calculated for the initial and the destination state of the move.

To ascertain that the biased Monte Carlo acceptance probability satisfies the condition of microscopic reversibility, we carried out a simulation of freely-rotating phantom chains of  $10^8$  Monte Carlo steps. In the absence of torsional

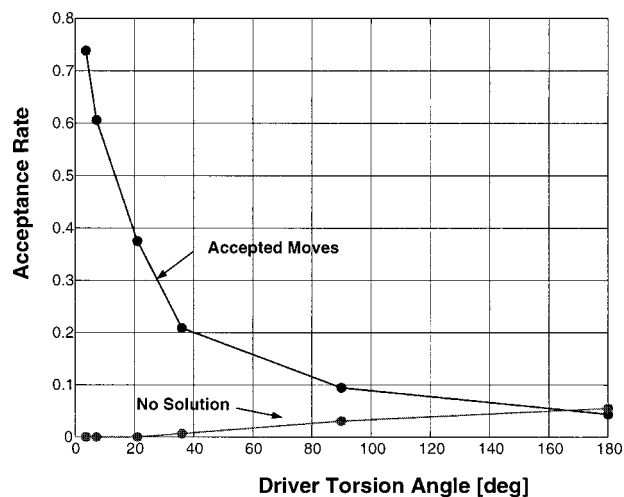


FIG. 5. Acceptance rate of Monte Carlo simulations of 20 chains of 24 beads for varying maximal amplitude of the changes in the driver angle of the ParRot move. The rate of geometric failure corresponds to the cases where the geometric ParRot problem has no solution (r.h.s. > 1).

potential and nonbonded interactions, an uniform distribution of dihedral angles must be expected. Figure 4 presents a comparison of the angle distribution obtained with biased and unbiased acceptance probability. Obviously, the geometric bias cannot be neglect, and is fully removed when considering the contribution  $J(n)$  to the acceptance probability criterion.

### III. MONTE CARLO SIMULATIONS

The present work aims at comparing the ParRot method to existing off-lattice Monte Carlo techniques. For that purpose, ParRot is supplemented with three Monte Carlo moves: (i) the Metropolis move (MMC) consists of a random displacement of the position and orientation of the chain simultaneously to random changes in the torsion angles of the chain backbone; (ii) the Continuum-Configurational-Bias method (CBMC) (Refs. 4 and 5) consists of a ‘‘cut’’ at a random position of a chain end and its step-by-step regrowth; (iii) the Reptation move<sup>1</sup> consists in the removal of the bond at a randomly selected end of the chain, and its regrowth at the other end of the chain. For a comprehensive review of these moves, see Leontidis *et al.*<sup>9</sup> No comparison was made with the Concerted-Rotation method,<sup>7-9</sup> since this method does not affect the chain ends and prohibits center-of-mass diffusion.

Our results were obtained with polybead molecules in the united atom approximation. These are chains formed by beads connected by rigid bonds of length 1.53 Å. The bond angle between successive bonds of a chain is fixed at 112°. The torsional potential energy function used, originally introduced by Ryckaerts and Bellemans,<sup>14</sup> is

$$U_{\text{tors}}(\phi) = C \sum_{n=0}^5 \alpha_n \cos^n \phi \quad (11)$$

with constant coefficients  $C = 9.27$  kJ/mol,  $\alpha_0 = 1$ ,  $\alpha_1$

TABLE I. Average properties over simulations of combined Monte Carlo techniques in 20 C<sub>24</sub>, 10 C<sub>71</sub>, and 9 C<sub>100</sub>.

	20 C <sub>24</sub>	10 C <sub>71</sub>	9 C <sub>100</sub>
<i>T</i> (K)	473	513	513
$\langle \rho \rangle$ (g cm <sup>-3</sup> )	0.62 ± 0.01	0.66 ± 0.03	0.67 ± 0.01
$\langle R_{\text{EED}}^2 \rangle / \langle R_G^2 \rangle$	8.08 ± 0.05	7.22 ± 0.26	6.41 ± 0.15

= 1.31,  $\alpha_2 = -1.414$ ,  $\alpha_3 = -0.3297$ ,  $\alpha_4 = 2.828$ ,  $\alpha_5 = -3.3943$ .<sup>15</sup> By this, the skeletal torsion angles are biased to favor *trans* and *gauche* states.

Sites on different chains and those on the same chain separated by more than three bonds interact through a non-bonded Lennard-Jones interaction function,

$$U_{\text{LJ}} = 4\varepsilon_{ij} \left\{ \left( \frac{\sigma_{ij}}{r_{ij}} \right)^{12} - \left( \frac{\sigma_{ij}}{r_{ij}} \right)^6 \right\}. \quad (12)$$

The energy-depth parameter  $\varepsilon_{ij} = \varepsilon = 0.41$  kJ/mol is the same for end-beads and middle-beads, and the bead size is set to  $\sigma = 3.94$  Å. These values have been found to reproduce *pVT* data of short polyethylenes.<sup>5</sup> Here, quantitative agreement between *pVT* data and simulation is not sought and we treat, therefore, the energy model in a simplified form, i.e., with a cutoff at  $2.5\sigma$  and no tail correction.

The simulations have been performed using a cubic box in an isothermal–isobaric simulation (*NpT*-simulation) at a pressure of 1 bar, following the procedure of Boyd.<sup>16</sup> Volume fluctuation moves were performed every 500 or 1000 moves, depending on the overall length of the simulation. An acceptance ratio of 20%–30% for the volume fluctuation move was obtained with a maximal amplitude change of the box side of 0.2 Å. The minimum image convention was used in all the simulations.

Three different polybead melts were investigated: a system of 20 chains of 24 beads each at 473 K (20 C<sub>24</sub>), a melt of ten chains of 71 beads each (10 C<sub>71</sub>) at 513 K and a melt of nine chains of 100 beads each (9 C<sub>100</sub>) at 513 K.

The new method of Müller *et al.*<sup>17</sup> was used to generate starting structures for the simulations. This method consists of a heuristic search algorithm in the space of torsion angles, which is capable of including configurational information in the structure generation and automatically delivers correct configurational statistics of the chains. The first 10<sup>5</sup> Monte Carlo steps were ignored in assessing the simulation results.

The *NpT* Monte Carlo simulations reported comprise 5 · 10<sup>6</sup> MC steps for 20 C<sub>24</sub> and 10 C<sub>71</sub>, and 2 · 10<sup>6</sup> or 3 · 10<sup>6</sup> MC steps for 9 C<sub>100</sub>. Thermodynamic quantities are summarized in Table I and II. Note that, due to the simplified energy model noted above, the agreement with experimental values cannot be perfect. The energies quoted in Table II are statistically identical and are reported only to show that the results of the simulations are not affected by substitution of ParRot for more traditional moves.

Table II shows the results of Monte Carlo runs for 10 C<sub>71</sub>. It is interesting to note that the fraction of accepted Monte Carlo moves is not strongly affected by the combination of moves. However, the ParRot move seems to benefit from cooperative effects among the moves as the relative large variation of its acceptance rate for different combinations of moves demonstrates.

The acceptance rate of the single moves is dependent on adjustable parameters such as, in the case of MMC, the amplitude of change in torsion angles, or, in the case of the CBMC method, the number of trial directions at each step of the regrowth. In the ParRot method, the only adjustable parameter is the maximum displacement  $\Delta\phi_0$  of the driver angle  $\phi_0$ . While a smaller value of  $\Delta\phi_0$  leads to higher acceptance rates of the ParRot moves, a larger value produces larger steps through the configuration space. Trial runs of 20 C<sub>24</sub> demonstrate that the acceptance ratio can readily be controlled by adjusting  $\Delta\phi_0$  (see Fig. 5). The acceptance rate of ParRot typically ranges from 5% to 75% according to the amplitude of  $\Delta\phi_0$ . ParRot also involves a more subtle effect of geometric nature. Larger amplitude  $\Delta\phi_0$  increases the number of geometric failures because it is more likely to encounter cases where the number of solutions of the ParRot equations falls to zero. However, Fig. 5 clearly demonstrates that the geometric failure level never exceed 6%. Further simulations involving ParRot moves were carried out with  $\Delta\phi_0 = 36^\circ$  resulting in an acceptance ratio of about 20%. The parameters for the other methods have been consistently kept constant in all simulations.

While the sampling ability of Monte Carlo techniques is most relevant, their computational efficiency also contributes to their overall performance. The relative CPU efficiency compares the average number of moves performed in the CPU time required for a CBMC move and is summarized for Reptation and ParRot in Table III. A CBMC move undoubtedly requires more computational effort than the other

TABLE II. Results obtained with different combinations of Monte Carlo techniques in isothermal–isobaric Monte Carlo simulations of 10 C<sub>71</sub> at 513 K and 1 bar. The simulations comprise 5 × 10<sup>6</sup> MC steps each. Thermodynamic properties and computational speed are compared. All simulations have been carried out on a Silicon Graphics workstation of type Octane (R10000).

Combination of move (%)				Accepted moves (%)				Properties		
MMC	Reptation	CBMC	ParRot	MMC	Reptation	CBMC	ParRot	MC steps s <sup>-1</sup>	$\langle E_{\text{tot}} \rangle$ (kJ/mol)	$\langle E_{\text{tors}} \rangle$ (kJ/mol)
10	30	30	30	4.3	14.3	6.1	18.0	20.7	17.3 ± 228.2	2648.6 ± 87.2
10	10	10	70	4.2	14.3	5.8	17.9	24.7	-14.9 ± 243.0	2629.5 ± 85.4
10	10	70	10	3.6	13.8	6.0	22.1	15.8	40.7 ± 202.5	2675.5 ± 85.5
10	70	10	10	5.6	17.8	6.6	23.7	24.6	47.8 ± 254.6	2626.5 ± 81.5
10	40	40	10	3.1	13.4	6.0	17.6	18.8	-72.0 ± 193.8	2638.1 ± 86.2
10	40	10	40	2.8	12.7	5.9	17.4	23.1	-105.0 ± 161.8	2657.4 ± 88.6
10	10	40	40	4.1	14.3	6.1	18.1	22.0	27.1 ± 256.8	2655.2 ± 91.0

TABLE III. Average number of MC steps performed during the time necessary for a CBMC step. All simulations have been carried out on Silicon Graphics workstations of type Octane (R10000).

	20 C <sub>24</sub>	10 C <sub>71</sub>	9 C <sub>100</sub>
CBMC (MC step)	1.0	1.0	1.0
Rept (MC step)	1.71	1.89	1.26
ParRot (MC step)	1.73	2.06	1.8

moves. It also appears that ParRot and Reptation use computational resources roughly equally.

#### IV. SAMPLING EFFICIENCY

To demonstrate the relative sampling ability in the space of dihedral angles, two simulations were performed on a system of 10C<sub>71</sub>. In both simulations, the elementary MMC move (10%) accompanies either Reptation moves (90%) or ParRot moves (90%). Beginning with the same initial structure, the occurrence densities of dihedral angles were calculated for both runs, with  $5 \cdot 10^6$  MC attempts each and a sampling frequency of 2000 MC attempts. Figure 6 shows these distributions. Since the number of MC attempts employed suffices for Reptation to attain proper sampling of all the bonds in the chains during simulation (the middle bonds are typically moved after  $1 \cdot 10^6$ ), the distribution obtained with Reptation constitutes a benchmark for other moves. As required, the distribution obtained with ParRot converges to the same form and shows, in addition, a smoothness that indicates a robust aptitude to efficiently sample the space of torsional degrees of freedom.

A first reason for the robust behavior of ParRot resides in the fact that three to four dihedral angles are simultaneously involved in a move. A second reason might be the amplitude of changes of the dihedral angles of the moving units, namely,  $\Delta\phi_0$ ,  $\Delta\phi_1$ ,  $\Delta\phi_2$ , and  $\Delta\phi_3$ . Figure 7 presents the distributions of these  $\Delta\phi$  for the accepted ParRot moves in simulations of 20C<sub>24</sub>, 10C<sub>71</sub>, and 9C<sub>100</sub> in runs

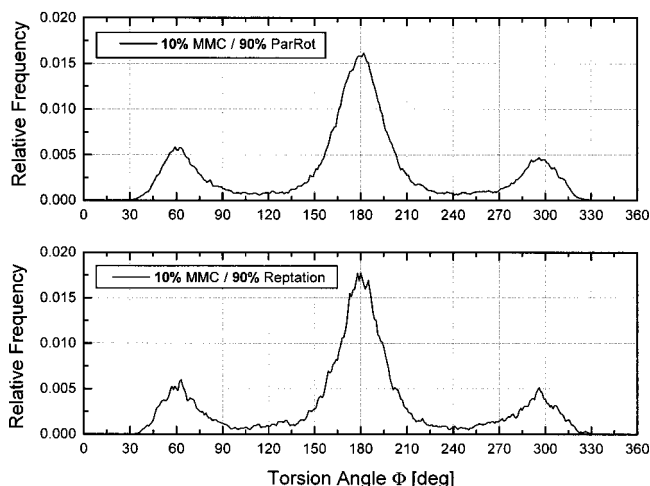


FIG. 6. Distributions of dihedral angles obtained in simulations of 20C<sub>24</sub> for mixtures of ParRot and MMC moves, and Reptation and MMC moves, respectively. The total number of MC steps is  $5 \cdot 10^6$ , and every two thousandth configuration has contributed to the distribution statistics.

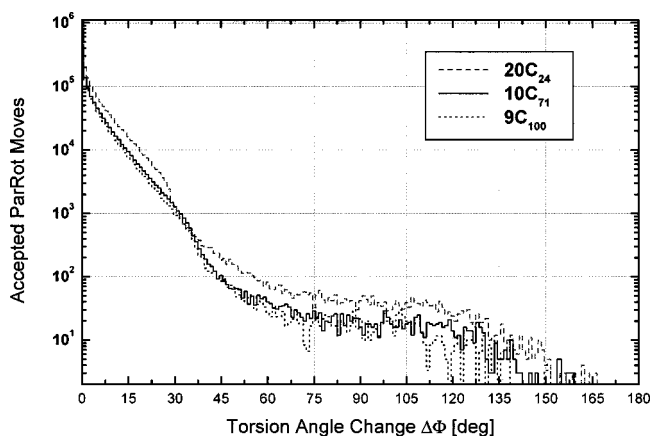


FIG. 7. Distribution of changes in torsion angles  $\phi_1$ ,  $\phi_2$ , and  $\phi_3$  for accepted ParRot moves in simulations of  $3 \cdot 10^6$  MC steps of 20C<sub>24</sub>, 10C<sub>71</sub>, and 9C<sub>100</sub>.

carried out with 10% MMC, 10% Reptation, 10% CBMC, and 70% ParRot moves. We observe in Fig. 7 that most changes in dihedral angle  $\Delta\phi$  range from  $0^\circ$  to  $45^\circ$ . However, a small number of ParRot moves results in larger changes in dihedral angles with amplitudes up to  $150^\circ$ . Slightly different distributions are characteristic for systems with different chain lengths.

Figure 8 provides a comparison between simulations where the maximum changes in the driver angle were  $\Delta\phi = 36^\circ$  and  $\Delta\phi = 180^\circ$ , respectively. As one might expect, simulations of 10C<sub>71</sub> and 9C<sub>100</sub> demonstrate that, on the one hand, an increase of the maximum amplitude  $\Delta\phi$  slightly decreases the number of accepted moves, but that, on the other hand, the tails of the distributions are only marginally affected by the amplitude  $\Delta\phi$ .

The effect of  $\Delta\phi$  on the ParRot move is clear when monitoring displacement amplitudes of the moved chain atoms. Figure 9 shows that typical atom displacements range from 0 to 1 Å. Remember that all atoms of the moving chain part are equally displaced in a ParRot move. In rare cases, the atom displacement can even attain more than 3 Å.

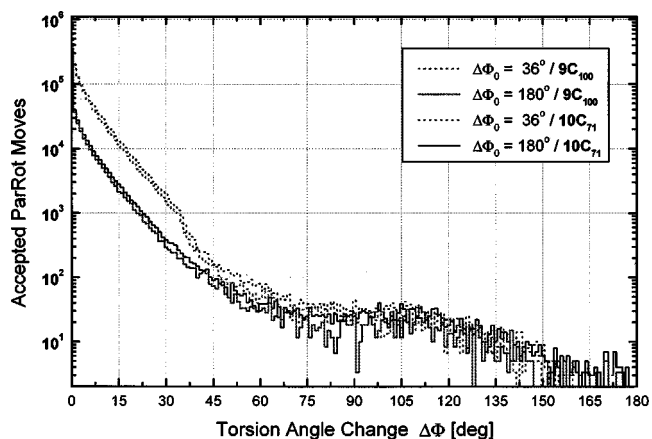


FIG. 8. Distribution of changes in torsion angles  $\phi_1$ ,  $\phi_2$ , and  $\phi_3$  for accepted ParRot moves in simulations of  $3 \cdot 10^6$  MC steps of 10C<sub>71</sub> and 9C<sub>100</sub>. The maximal amplitude of change in the driver torsion angles has been taken to be  $\Delta\phi_0 = 36^\circ$  and  $\Delta\phi_0 = 180^\circ$ .

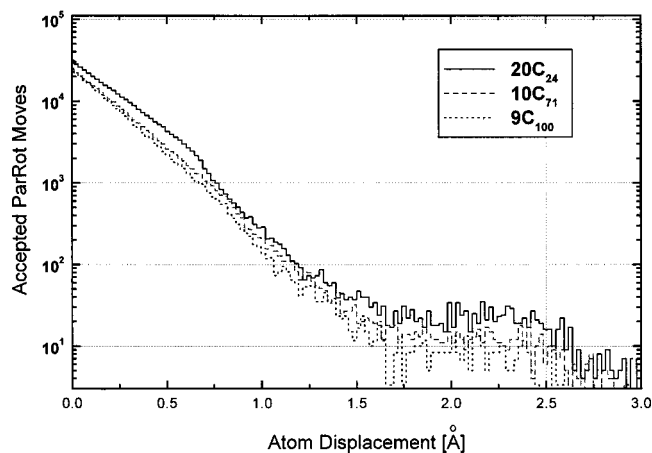


FIG. 9. Distribution of displacements of the moving chain end for accepted ParRot moves in simulations of  $3 \cdot 10^6$  MC steps of 20  $C_{24}$ , 10  $C_{71}$ , and 9  $C_{100}$ .

Figure 10 shows how the displacement of atoms varies if ParRot is used together with other techniques in  $10C_{71}$ . Even though the combination 10% MMC, 30% Reptation, 30% CBMC, 30% ParRot comprises less ParRot attempts than a simulation purely based on ParRot, the fraction of accepted ParRot moves is still larger than in the case where the maximum driver amplitude  $\Delta\phi$  was increased to  $180^\circ$ .

Efficient sampling of the torsional degrees of freedom of chains requires all the dihedral angles to be relaxed during simulation. It becomes a particularly difficult task for dihedral angles deep within the chains. For instance, MMC performs poorly in that case because, due to leverage effects, only tiny changes in dihedral angles can lead to reasonable acceptance rates.

In order to assess the capability to relax dihedral angles within the chains, the number of accepted ParRot attempts for each bonds chosen as driver angle can be counted. A simulation of long chains ( $9C_{100}$ ) depicted in Fig. 11 demonstrates that the acceptance of ParRot moves is hardly affected by the location of the moving unit. About half as many ParRot moves are accepted for dihedral angles in the middle of the chain than for those at the extremities. To our

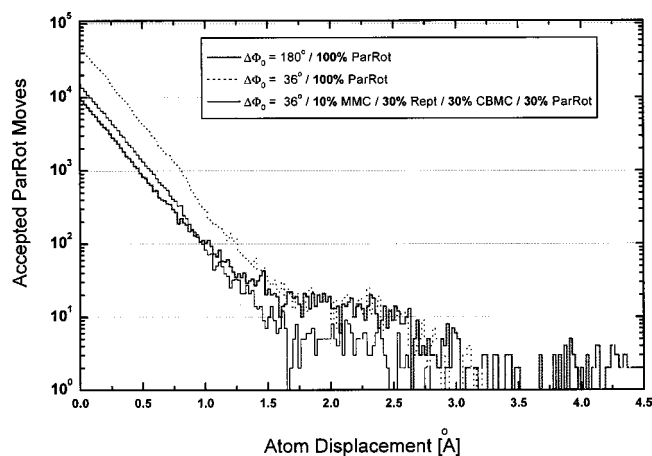


FIG. 10. Distribution of accepted ParRot moves for varying  $\Delta\phi_0$  of the driver torsion angle in simulations of length  $3 \cdot 10^6$  MC steps on 9  $C_{100}$ .

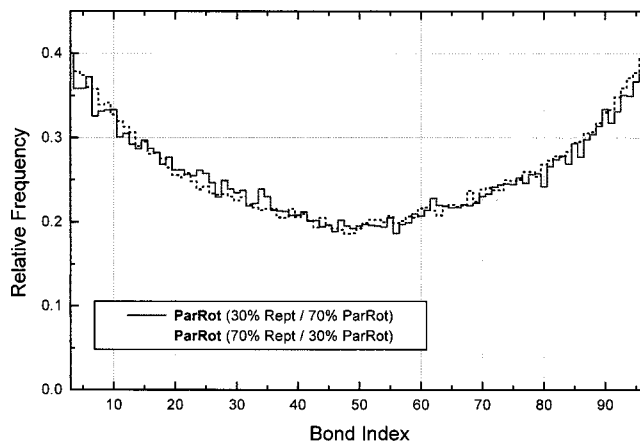


FIG. 11. Distribution of accepted moves at each bond within the chain in simulations of length  $3 \cdot 10^6$  MC steps of 9  $C_{100}$ .

knowledge, none of the presently existing off-lattice Monte Carlo methods is capable to sample so efficiently all torsional degrees of freedom regardless of their position within long chains.

A similar assessment has been made for  $10C_{71}$  (see Fig. 12). Here the distribution of CBMC moves has been included (the depth of the cut has been tracked). Due to the shorter chains, the relative decrease of accepted ParRot moves between the middle and the end of the chains is not as pronounced as in  $9C_{100}$ . The performance of the CBMC method clearly worsens when handling bonds deeper in the chains and is only practical for the terminal dozen bonds or so; it decreases exponentially with the number of bonds for regrowth.

The mean-square displacement of the center-of-mass of the chains  $\langle r_{c.o.m.}^2 \rangle$  constitutes a criterion of long-time and long-distance performance of simulation techniques. ParRot alone provides little towards displacing the center-of-mass of the chains (Figs. 13 and 14). Introducing Reptation dramatically improves performance and a balanced mixture of Reptation/ParRot satisfactorily competes with the Reptation/ParRot/CBMC combination. In both figures, combinations

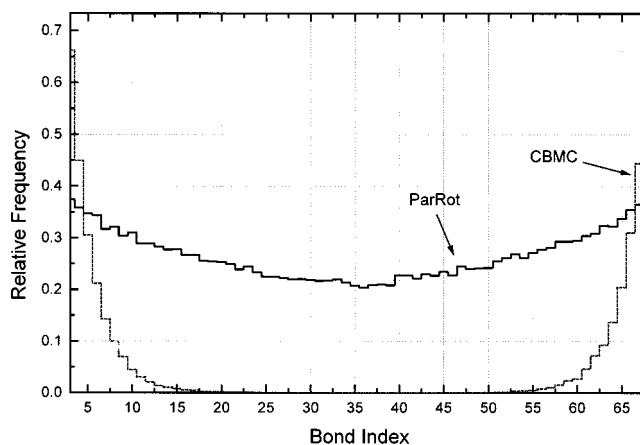


FIG. 12. Distribution of accepted moves at each bond within the chain in simulations of length  $3 \cdot 10^6$  MC steps of 10  $C_{71}$ .

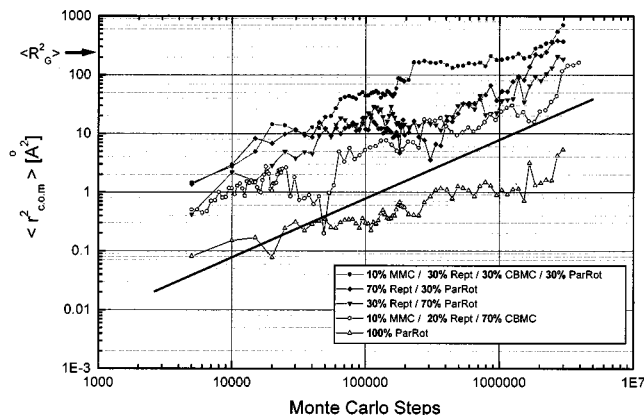


FIG. 13. Diffusion of the centers of mass of the chains in simulations of 9  $C_{100}$  obtained with different combinations of Monte Carlo techniques. The straight line is of unit slope and serves as a guide.

without ParRot were among the worst performing mixtures of moves tested.

## V. CONCLUSIONS

The novel off-lattice ParRot method has been demonstrated to be suitable for the isothermal–isobaric simulation of atomistically detailed dense polymer systems, especially for long chains at high density. ParRot operates on the entire chain in contrast to most continuum MC methods that operate only on the chain ends or the chain interior. Solutions finding is extremely simple because the geometric problem stated in Parallel Rotation can be solved analytically. Consequently the ParRot technique proved to be computationally very efficient.

Furthermore the ParRot technique can be used for polymer chains of arbitrary chemical structure. Since ParRot considers four consecutive dihedral angles without attention to the molecular structure between these “joints,” it can be

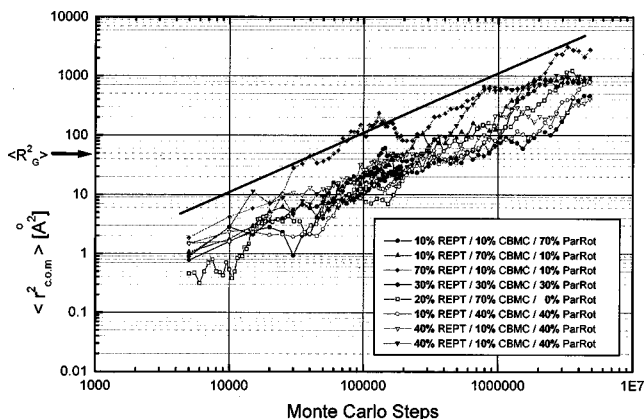


FIG. 14. Diffusion of the centers of mass of the chains in simulations of 10  $C_{71}$  obtained with different combinations of Monte Carlo techniques. The straight line is of unit slope and serves as a guide.

applied to structures with pendant groups, or even branching structures and to systems with arbitrary bond lengths, angles, and monomer-unit sizes.

The ParRot algorithm permits changing torsion angles and displacing large chain segments that are deeply inside long chains in dense polymeric system. ParRot enables efficient changes of dihedral angles in the moving unit of up to  $120^\circ$  and enables the displacements of atoms in the moving chain end of up to  $1.5 \text{ \AA}$ . The number of accepted ParRot moves is hardly affected by the depth of the variable unit in the chains. Even in systems with the longest chains investigated here ( $C_{100}$ ), the number of successful ParRot attempts in the middle of the chains was about half of that at the chain ends. ParRot thus provides a most appropriate technique for efficiently sampling all dihedral angles. The Monte Carlo acceptance rate of the new elementary move is not very sensitive to the maximal amplitude of change of the driver torsion angle and can be adjusted to a broad range of values: from 5% up to 75%.

Special considerations are required in designing the acceptance criterion of the elementary MC move in order to satisfy the principle of detailed balance in MC methods. Tests prove that this acceptance criterion is correct.

ParRot predominantly addresses the issue of moving all torsion angles in a chain, but is inefficient in displacing the chains as a whole. Large rates for the diffusion of the centers of mass of the chains can only be obtained when balanced combinations of various Monte Carlo techniques are used.

## ACKNOWLEDGMENT

We gratefully acknowledge the financial support provided by the Swiss National Science Foundation (Schweizerischer Nationalfonds zur Förderung der Wissenschaftlichen Forschung).

- <sup>1</sup>P. G. de Gennes, *J. Chem. Phys.* **55**, 572 (1971).
- <sup>2</sup>M. Bishop, D. Ceperley, H. L. Frisch, and M. H. Kalos, *J. Chem. Phys.* **72**, 3228 (1980).
- <sup>3</sup>M. Vacatello, G. Avitabile, P. Corradini, and A. Tuzi, *J. Chem. Phys.* **73**, 548 (1980).
- <sup>4</sup>J. Siepman and D. Frenkel, *Mol. Phys.* **75**, 59 (1992).
- <sup>5</sup>J. J. de Pablo, M. Laso, and U. W. Suter, *J. Chem. Phys.* **96**, 6157 (1992).
- <sup>6</sup>A. Widmann and U. W. Suter, *Comput. Phys. Commun.* **92**, 229 (1995).
- <sup>7</sup>N. Go and H. A. Scheraga, *Macromolecules* **3**, 178 (1970).
- <sup>8</sup>L. R. Dodd, T. D. Boone, and D. N. Theodorou, *Mol. Phys.* **78**, 961 (1993).
- <sup>9</sup>E. Leontidis, J. J. de Pablo, M. Laso, and U. W. Suter, *Adv. Polym. Sci.* **116**, 285 (1994).
- <sup>10</sup>P. J. Flory, *Macromolecules* **7**, 381 (1974).
- <sup>11</sup>W. F. Van Gunsteren and M. Karplus, *Macromolecules* **15**, 1528 (1982).
- <sup>12</sup>W. L. Mattice and U. W. Suter, *Conformational Theory of Large Molecules* (Wiley, New York, 1994).
- <sup>13</sup>K. Binder, *Monte Carlo Simulations in Statistical Physics* (Springer, Berlin, 1992).
- <sup>14</sup>J. P. Ryckaert and A. Bellemans, *Chem. Phys. Lett.* **30**, 123 (1975).
- <sup>15</sup>D. Rigby and R.-J. Row, *J. Chem. Phys.* **87**, 7285 (1989).
- <sup>16</sup>R. H. Boyd, *Macromolecules* **22**, 2477 (1989).
- <sup>17</sup>M. Müller, S. Santos, J. Nievergelt, and U. W. Suter, *J. Chem. Phys.* **114**, 9764 (2001), preceding paper.